

Graphene supports the manipulating multiple mode propagation in the hybrid plasmonic waveguides

JICHENG WANG^{a,b,*}, XIAOSAI WANG^a, ZHENG-DA HU^a, CI SONG^a, SHUTIAN LIU^b

^a*School of Science, Jiangsu Provincial Research Center of Light Industrial Optoelectronic Engineering and Technology, Jiangnan University, Wuxi 214122 China*

^b*Department of Physics, Harbin Institute of Technology, Harbin 150001, China*

A new type of plasmonic waveguide based on a graphene-coated V-groove structure which can achieve better subwavelength confinements and longer propagation compared to the conventional metal waveguide is proposed. By dynamically altering the chemical potential of graphene, graphene surface plasmon polaritons (GSPPs) multiple modes of the hybrid graphene-coated waveguide can be reached. And the mode field energies can be well confined in the V-groove or the waveguide. The mode confinement becomes weaker and the propagation length gets longer as the chemical potential of graphene increasing. In addition, the mode propagation can be changed by adjusting the radius of the waveguide and the frequencies and the higher mode is achieved at the same time. The finite element method (FEM) has been employed to study the mode distributions and electromagnetic responses of our designs at mid-infrared frequencies. Those proposed structures may pave a way for the further development of ultra-compact, fast-tunable and long-propagation devices in the infrared region (IR).

(Received May 31, 2016; accepted November 25, 2016)

Keywords: Graphene plasmonics, Mode propagation, Hybrid waveguide, FEM

1. Introduction

Surface plasmon polaritons (SPPs) are electromagnetic surface waves that exist at the interface between metal and dielectric with an exponential decay perpendicular to the surface on both sides [1, 2]. This unique property of SPPs provides a way to manipulate light with subwavelength confinement [3-7]. A great deal of attention have been devoted to researches in highly integrated photonic circuits [8-10], nanofocusing [11], optical metamaterials [12], nanophotonic lasers [13], biochemical sensor [14], amplifiers [15]. Various kinds of plasmonic waveguide structures [16-20] such as metal groove waveguides [21-23], wedge waveguides [24] have been proposed to realize the confinement and propagation of light. However, these metal structures suffer high propagation losses and they are difficult to vary the permittivity of the noble metal such as gold to decrease the material losses. Compared to the noble metal, graphene has been thoroughly researched as a promising platform for highly integrated plasmonic circuits during recent years due to its remarkable optical properties, such as extreme confinement, dynamic tunability and low losses [25-36]. Especially, the surface conductivity of graphene could be dynamically tuned by electrochemical potential via gate voltage, electric fields, magnetic fields, and

chemical doping. Graphene surface plasmon polaritons (GSPPs) modes [37-39] have been investigated in the terahertz ranges as well. Furthermore, it has been proved by several experiments that graphene layer can be tightly coated on the dielectric nanowaveguide [40, 41].

In this paper, we propose a graphene-coated hybrid plasmonic waveguide analogous to the channel plasmon polaritons (CPPs) based on the graphene-coated V-groove and nanowire in the terahertz frequency. By using the Finite Element Method (FEM) [42], the graphene plasmonic modes are numerically calculated and the dispersion relation as well as propagation length of these modes are illustrated. Furthermore, the dependence on the chemical potential of graphene and waveguide radius is investigated as well.

2. Methods

The two-dimensional numerical simulations are carried out in the configurations using the FEM. The surface conductivity of graphene σ_s , is governed by the Kubo formula including the interband and intraband transition contributions:

$$\sigma_s = \frac{ie^2\mu_c}{\pi\hbar^2(\omega+i\tau^{-1})} + \frac{ie^2}{4\pi\hbar} \ln \left[\frac{2\mu_c - (\omega+i\tau^{-1})\hbar}{2\mu_c + (\omega+i\tau^{-1})\hbar} \right] + \frac{ie^2k_B T}{\pi\hbar^2(\omega+i\tau^{-1})} \ln \left[\exp\left(-\frac{\mu_c}{k_B T}\right) + 1 \right] \quad (1)$$

It depends on temperature T , chemical potential μ_c , momentum relaxation time τ , and photon frequency ω . Here, e is the electron charge. In graphene, the dependence of momentum relaxation time τ on the carrier mobility μ can be described as $\tau = \mu\mu_c / (e\nu_f^2)$. The carrier mobility μ is temperature dependent and reasonably chosen to be $\mu = 20000 \text{ cm}^2\text{V}^{-1}\text{s}^{-1}$ from experiment results at room temperature [33]. In our analysis, the employed incident light is in the mid-infrared range where the intraband transition contribution dominates in monolayer graphene. Under this condition, the optical conductivity can be simplified to:

$$\sigma_g(\omega) = \frac{ie^2\mu_c/\pi\hbar^2}{\omega + i\tau^{-1}} \quad (2)$$

Here, τ is assumed to be 0.5 ps. The equivalent permittivity of graphene is given by the equation [25]:

$$\varepsilon_{g,eq} = 1 + \frac{i\sigma_g\eta_0}{k_0\Delta} \quad (3)$$

where $k_0 = 2\pi/\lambda$ is wavenumber in vacuum and $\eta_0 \approx 377 \Omega$ is the intrinsic impedance of air. The thickness of graphene layer coated on the V-groove and waveguide is assumed as $\Delta = 0.5 \text{ nm}$. The monolayer graphene support TM-polarized surface plasmon polaritons is only in consideration for the investigation. The dispersion relation of this TM SPP surface wave follows the equation:

$$\beta_{spp} = k_0 \sqrt{1 - \left(\frac{2}{\eta_0\sigma_g} \right)^2} \quad (4)$$

where β_{spp} is the propagation constant of graphene surface plasmon polaritons. The effective refractive index of GSPPs shows the ability to confine SPPs on graphene, which is defined as $N_{eff} = \beta_{spp}/k_0$. The propagation length is defined as $L = 1/2\text{Im}(\beta_{spp})$ featuring the SPP propagation loss in graphene. Furthermore, it should be noted that the dispersion relation of GSPPs on monolayer graphene works on graphene rings as well. The relationship of $\text{Re}(N_{eff})$ and L on the chemical potential μ_c and incident light wavelength λ are shown in Fig. 1. Obviously, from Fig. 1a, $\text{Re}(N_{spp})$ increases as the chemical potential μ_c decreases for a fixed wavelength, which means that GSPPs are better confined at a lower chemical potential. Nevertheless, the tendency in Fig. 1b is evidently opposite to that in Fig. 1a, indicating that a lower chemical potential gives a smaller propagation length. Therefore, both the

two factors could play an important role on the mode patterns in our proposed structures. In this paper, we consider the GSPPs modes in the frequency ranges from 10 to 50 THz neglecting the influence of optical phonon at the whole frequency range and the chemical potential ranges from 0.1 to 1.0 eV where TE mode will not occur.

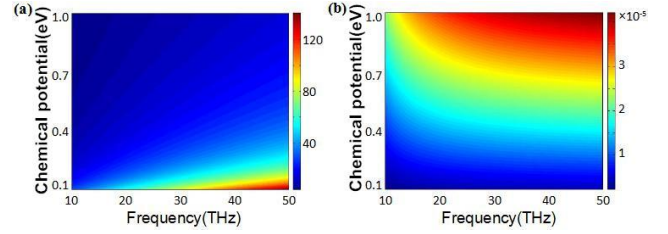


Fig. 1. The real part of effective refractive index and the propagation length for GSPPs versus frequency and chemical potential. (a) Real part of effective refractive index for GSPPs and (b) propagation length L_{spp} as a function of frequency and chemical potential

The three-dimensional structure of the hybrid waveguide is depicted in Fig. 2a with relevant parameters denoted in it. θ is the opening angle of the V-groove, d is the depth of the V-groove, r is the radius of the waveguide. In the structure, the blue part represents graphene, and the yellow part represents substrate with permittivity ε . The Cartesian coordinate system is shown in the inset. The proposed structure is excited with a plane wave propagating along the z axis. In order to fully understand the mode propagation in the graphene-coated hybrid plasmonic waveguide, the graphene-coated V-groove and the graphene-coated nanowire are both discussed in the following paper. For simplicity, our calculations consider all the structures embedded in air.

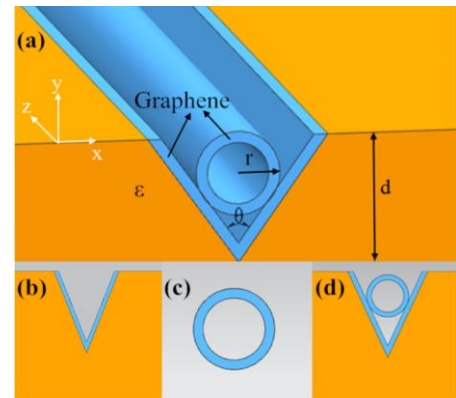


Fig. 2. Schematic of the proposed structures. (a) Tomograph of the graphene-coated hybrid plasmonic nanowaveguide. The GSPPs propagate along the z axis. Relevant parameters are denoted above. (b), (c), and (d) are schematic of graphene-coated V-groove, graphene-coated nanowire and the hybrid plasmonic nanowaveguide respectively

3. Results and discussion

3.1. Surface plasmon modes in graphene-coated V-groove

The structure of the graphene-coated V-groove is presented in Fig. 2b, where the graphene sheet is laid on the top surface of the groove substrate. The opening angle of the groove θ is set to 20° , and the depth of the groove is $d = 300$ nm. Compared to the conventional CPPs mode supported by the noble metal, the graphene-coated V-groove mode is mostly confined in the groove under these conditions. And the loss caused by metal dissipations is zero which leads to a longer propagation length. One of the special optical properties of graphene is that the graphene conductivity could be dynamically tuned by changing chemical potential μ_c . Fig. 3b presents the effective index of the plasmonic modes in the graphene-coated V-groove waveguide as a function of chemical potential μ_c ranges from 0.2 to 1.0 eV. As shown in Fig. 3b, the effective mode index decreases with chemical potential increasing, which can be explained from Eq. (4) and matches well with Fig. 1a. This suggests that the modes become less localized in the groove and the propagation losses decrease. As a result, the propagation lengths of the plasmonic modes in the graphene-coated V-groove waveguide enlarge with the chemical potential increasing as depicted in Fig. 3b. The mode fields are almost confined in the V-groove structure as shown in Fig. 3a. When the chemical potential μ_c changes from 0.2 to 1.0 eV, the mode field energies of the bottom becomes weaker. The results of the data from Fig. 3b and Fig. 3c match well with those in Fig. 3a.

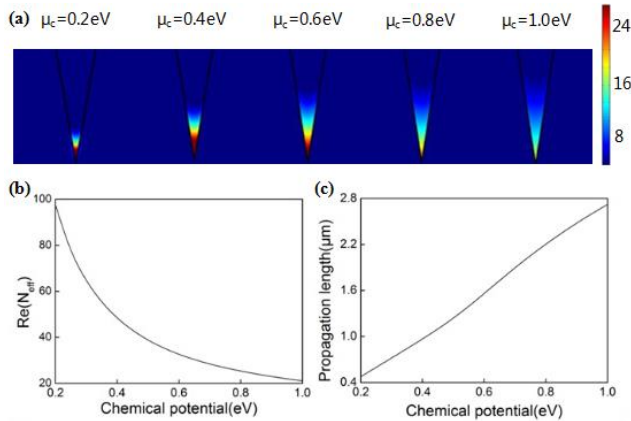


Fig. 3. Mode distributions at different chemical potential. (a) The electric field energy at different chemical potential (0.2, 0.4, 0.6, 0.8, and 1.0 eV), (b) the real part of effective index and (c) the propagation length of the plasmon modes in the V-groove waveguide as a function of chemical potential of graphene with $\theta = 20^\circ$, $d = 300$ nm and $f = 30$ THz

By increasing the opening angel of the groove to 25° , the chemical potential μ_c being set as 0.5 eV, the depth $d = 1$ μm and other parameters remaining the same, we can

achieve the mode distributions of the first 5 order modes. It is exhibited in Fig. 4 showing the electric field E_z , the electric field norms and the charge orderings for the GSPPs in the V-groove. The mode field energy almost localizes in the interface of graphene and substrate, showing a strong mode confinement. On the other hand, this symmetrical V-groove can be regarded as the graphene ribbon, where m is the mode number. When $m = 0$, there are only positive charges dispersed outward. $m = 1$ represents there are a pair of opposite charges starting at positive charges and ending at negative charges, $m = 2$ represents there are two pairs of opposite charges, and $m = 3, 4$ can be done with the same manner.

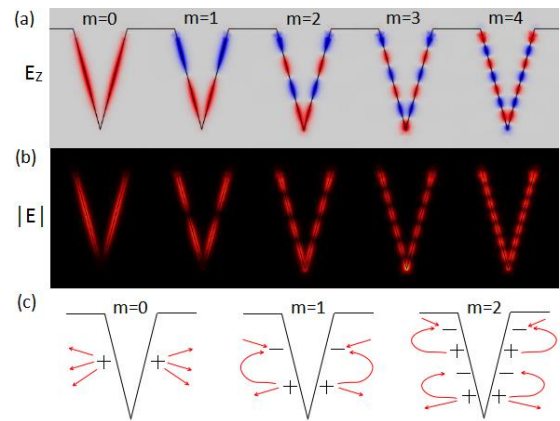


Fig. 4. Mode distributions of the first 5 order modes at $\theta = 25^\circ$ and $\mu_c = 0.5$ eV. (a) The electric field E_z , (b) the normalized electric field and (c) the charge orderings for the GSPPs in the V-groove

3.2. Surface plasmon modes in graphene-coated waveguide

The graphene-coated waveguide with the radius of $r = 300$ nm, which can be regarded as a graphene sheet wounded into a circle around a substrate with the permittivity of $\epsilon = 1$, is shown in Fig. 1c. Fig. 5a clearly demonstrates the GSPPs mode distributions of the 10th order modes at the chemical potential $\mu_c = 0.15$ eV. The number of supported surface plasmonic modes in the waveguide could be estimated as $m = 2\pi r N_{\text{eff}} / \lambda$. In the equation, λ is the EM wavelength in the free space. When $m = 0$, there is no standing wave in the waveguide. $m = 1$ represents there is a standing wave, $m = 2$ represents there are two standing waves, and $m = 3 - 9$ can be done in the same way. As shown in Fig. 5b, the effective mode index decreases with chemical potential increasing, which reveals the modes becomes less localized in the waveguide and the propagation loss becomes lower. This leads to the propagation length increasing as depicted in Fig. 5c. At $\mu_c = 0.38, 0.3, 0.26, 0.22, 0.18$ and 0.16 eV, $m = 4, 5, 6, 7, 8, 9$ order modes cut off respectively. Higher order mode does not exist at high doping level. This demonstrates single mode operation could be realized by simply changing chemical potential.

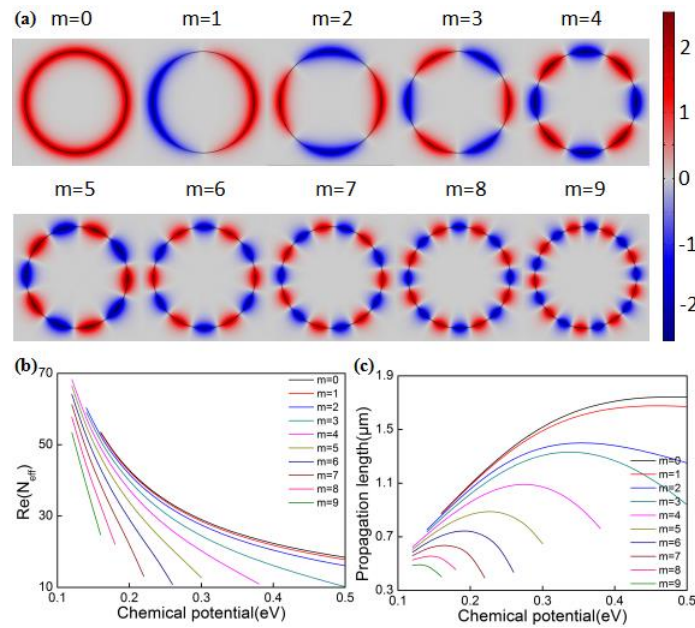


Fig. 5. Mode distributions at different chemical potential. (a) Mode distributions of the 10th modes at $\mu_c = 0.15$ eV with the permittivity $\epsilon = 1$, (b) the effective index and (c) the propagation length of the GSPPs modes in the waveguide as a function of chemical potential of graphene with $r = 300$ nm and $f = 30$ THz

The influences of radius and frequency on the mode propagation are also discussed. Fig. 6a shows the effective mode index decreases with the radius reducing. The propagation length has the same tendency as depicted in Fig. 6b. A significant reduction in the number of supported plasmonic modes in this waveguide could be seen in Fig. 6a with the decreasing of radius. The values of effective index at $m = 0$ and $m = 1$ modes are almost same. At radii of $r = 180, 200, 230$ and 250 nm, $m = 6, 7, 8, 9$ order modes cut off respectively. Fig. 6c,d show the impact of frequency on the effective mode index and the propagation

length in the waveguide. The radius is $r = 300$ nm and other parameters remain the same. The effective mode index decreases with the frequency increasing as shown in Fig. 6c. This suggests the modes become less localized in the waveguide as the frequency increasing, and the propagation loss gets lower. This leads to the propagation length increasing as depicted in Fig. 6d. At the frequency of 24, 20, 16, 14 and 12 THz, $m = 0, 1, 6, 7, 8$ order modes cut off respectively. And $m = 2, 3, 4, 5$ order modes cut off at the frequency of 18 THz.

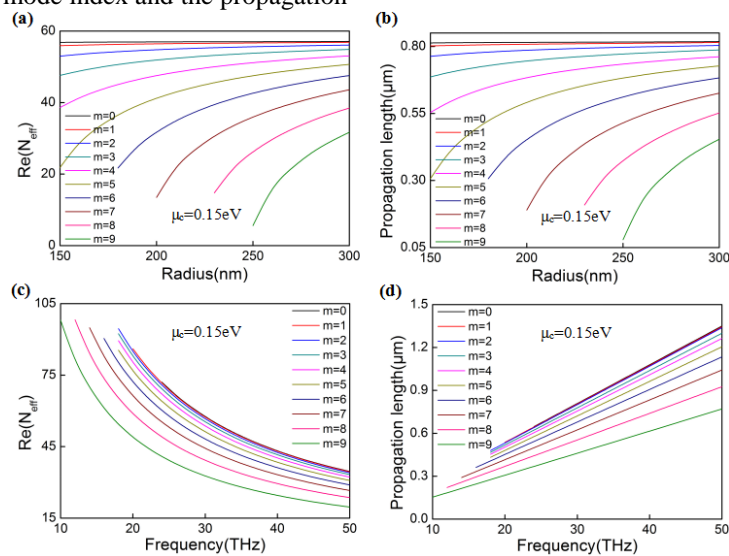


Fig. 6. The effective index and propagation length of the GSPPs in the waveguide versus radius and frequency with $\mu_c = 0.15$ eV. (a) The effective index and (b) the propagation length as a function of radius at $f = 30$ THz, (c) the effective index and (d) the propagation length as a function of frequency at $r = 300$ nm

The permittivity of the substrate in the graphene-coated waveguide also has an influence on the GSPPs mode distributions. Be similar to the influence on metal waveguide, higher the permittivity is, weaker the electric field to the interface between graphene and substrate is. By changing the permittivity of the substrate, high mode could exist in higher chemical potential. Here, for convenience, we set the permittivity $\varepsilon = 2$. The normalized electric field distributions of the 10th order

modes at the chemical potential $\mu_c = 0.5$ eV can be seen from Fig. 7a. The effective mode index and the propagation length at $\mu_c = 0.5$ eV have the same tendency to those at $\mu_c = 0.15$ eV by comparing Fig. 7b,c with Fig. 5b,c. However, in this condition, $m = 6, 7, 8, 9$ order modes cut off respectively when $\mu_c = 0.85, 0.75, 0.65$ and 0.55 eV, which is much larger than those at $\mu_c = 0.15$ eV discussed above. This reveals a stronger mode confinement and a larger propagation length.

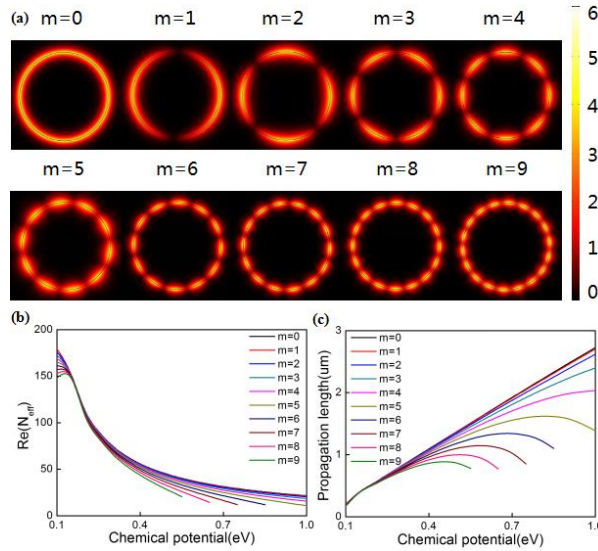


Fig. 7. Mode distributions at different chemical potential. (a) Mode distributions of the 10th modes in the waveguide at $\mu_c = 0.5$ eV with the permittivity $\varepsilon = 2$, (b) the effective index and (c) the propagation length of the GSPPs modes as a function of the chemical potential of graphene with $r = 300$ nm and $f = 30$ THz

The response of the effective index and the propagation length to the radius and frequency is also discussed with $\varepsilon = 2$ at $\mu_c = 0.5$ eV. As shown in Fig. 8 a,b, with the chemical potential increasing, the effective index

decreases and the propagation length increases which is consistent with Fig. 1. At radii of $r = 160, 190, 220$ and 250 nm, $m = 6, 7, 8, 9$ order modes cut off respectively.

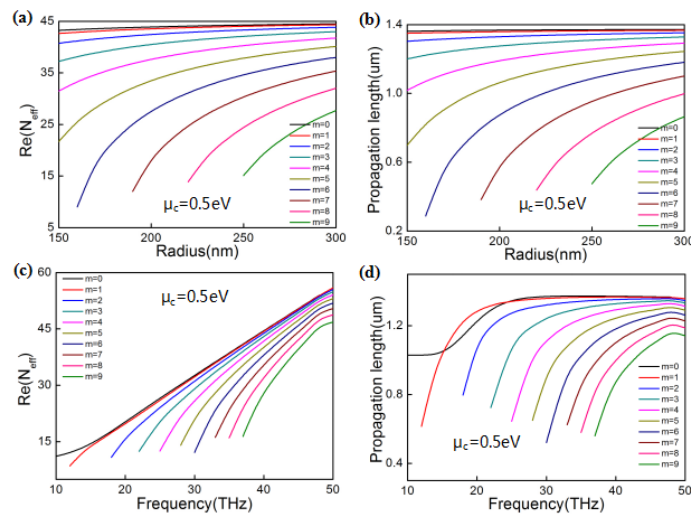


Fig. 8. The effective index and propagation length of the GSPPs in the nanowire versus radius and frequency with $\mu_c = 0.5$ eV. (a) The effective index and (b) the propagation length as a function of radius at $f = 30$ THz, (c) the effective index and (d) the propagation length as a function of frequency at $r = 300$ nm

3.3. Surface plasmon modes in the hybrid plasmonic waveguide

Based on the graphene-coated V-groove and the graphene-coated waveguide discussed above, we investigate the graphene-coated hybrid plasmonic waveguide. The cross section graph can be seen from Fig. 2d with $\theta = 25^\circ$, $d = 1 \mu\text{m}$ and $r = 160 \text{ nm}$. We assume the chemical potential in the waveguide and the V-groove are $\mu_{c1} = 0.2 \text{ eV}$ and $\mu_{c2} = 0.15 \text{ eV}$ respectively. The surface plasmon modes supported by the hybrid plasmonic waveguide is similar to those in the waveguide by comparing Fig. 9a and Fig. 5a. But the radius of the waveguide gets smaller in this case and the mode confinement is stronger. Therefore, the propagation length becomes longer.

Fig. 9b,c shows the effective index and the propagation length of the plasmon modes in the hybrid plasmonic waveguide respectively as a function of μ_{c1} (the

chemical potential in waveguide) with $\mu_{c2} = 0.15 \text{ eV}$ being set. Other parameters remain the same. With the chemical potential increasing, the effective index reduces while the propagation length increases. By comparing Fig. 9 with Fig. 5, we can get that the effective mode index and the propagation length in the hybrid plasmonic waveguide have the same tendency with these in the waveguide. The difference is only $m = 0, 1$ and 2 order modes are there in the hybrid graphene waveguide. Higher order modes do not exist in this condition with the chemical potential increasing. At $\mu_{c1} = 0.4 \text{ eV}$, $m = 2$ order mode cuts off. For $m = 1$ mode, the propagation length reaches a maximum value at $\mu_{c1} = 0.8 \text{ eV}$. What's more, the propagation length has a maximum value up to $5 \mu\text{m}$ at $m = 0$ mode. This demonstrates single mode operation could be realized by simply changing chemical potential and longer mode propagation could be reached.

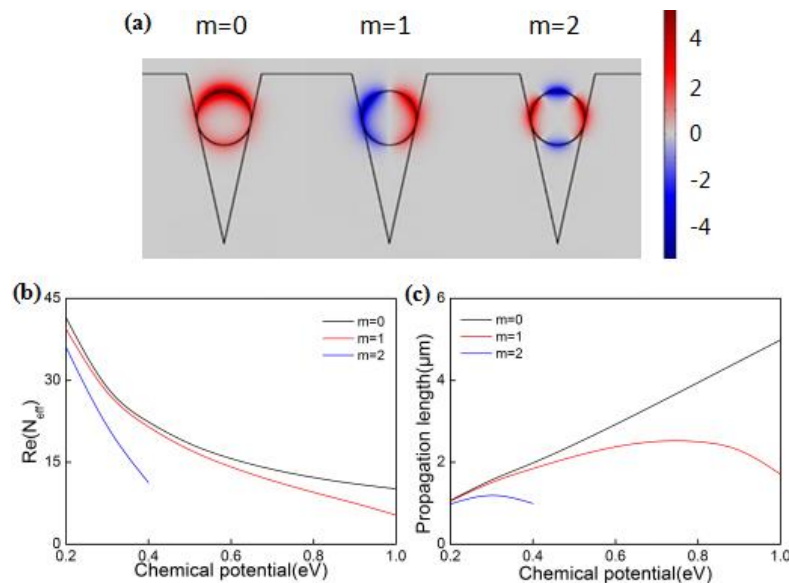


Fig. 9. Mode distributions at different chemical potential. (a) The mode distributions in the hybrid nanowaveguide of the first 3 order modes with $\theta = 25^\circ$, $d = 1 \mu\text{m}$ and $r = 160 \text{ nm}$, (b) the effective index and (c) the propagation length of the GSPPs modes in the structure as a function of μ_{c1} (the chemical potential in nanowire) with $\mu_{c2} = 0.15 \text{ eV}$ being set

Fig. 10a presents the surface plasmon mode patterns with $\theta = 25^\circ$, $d = 1 \mu\text{m}$ and $r = 160 \text{ nm}$ at $f = 30 \text{ THz}$. The mode area becomes larger at the bottom of the V-groove with the chemical potential in it increasing. It reveals that the mode confinement becomes weaker at the bottom of the groove. Fig. 10b shows the effective index of the plasmon modes in the hybrid plasmonic waveguide as a

function of μ_{c2} (the chemical potential in V-groove) with $\mu_{c1} = 0.2 \text{ eV}$. The effective mode index decreases with the chemical potential increasing, which leads to an increasing propagation length in this structure eventually as depicted in Fig. 10c.

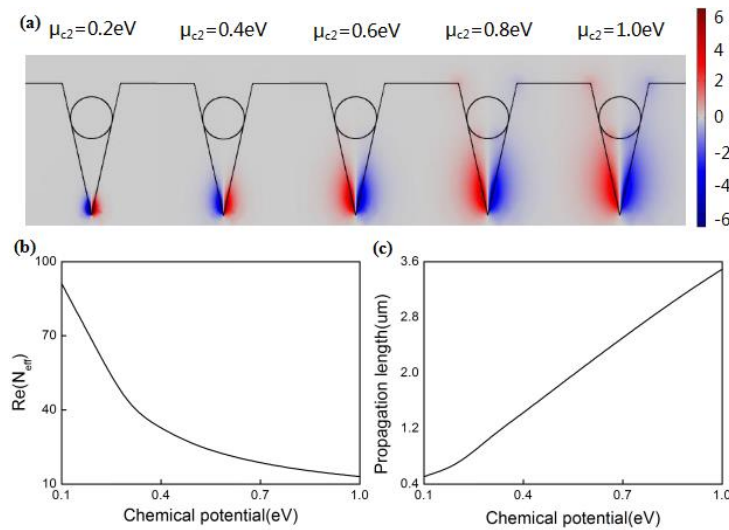


Fig. 10. Mode distributions at different chemical potential. (a) Mode distributions with $\theta = 25^\circ$, $d = 1\mu\text{m}$ and $r = 160\text{ nm}$ at $f = 30\text{ THz}$, (b) the effective index and (c) the propagation length of the GSPPs modes in the hybrid plasmonic nanowaveguide as a function of the chemical potential in V-groove with $\mu_{c1} = 0.2\text{eV}$ being set

4. Conclusions

In this paper, we discuss the manipulating mode propagation in the V-groove, waveguide and hybrid plasmonic waveguides supported by graphene with the FEM numerical simulation. The effective mode index and the propagation length can be obtained by the eigen equation for dispersion relation. The effective mode index decreases as the chemical potential increasing. With the chemical potential, radius of the waveguide and the frequency increasing respectively, the propagation length gets longer. Especially, the tunable conductivity of graphene increasingly promotes the development of active plasmonic devices including absorbers, polarizers, and transformation optical devices. The graphene-coated hybrid plasmonic waveguide analogous to the conventional CPP waveguide has its unique advantages. For example, it can support the propagation of multi-mode with low loss caused by metal dissipation and surface scattering. And it has a better mode confinement which is of great importance in high density photonic integration circuits. All those proposed structures may be beneficial for the further development of ultra-compact, fast-tunable and high-performance devices in the IR region.

Acknowledgment

This work is supported by the National Natural Science Foundation of China (Grant Nos. 11504139, 11504140), the Natural Science Foundation of Jiangsu Province (Grant Nos. BK20140167, BK20140128), and the Key Laboratory Open Fund of Institute of Semiconductors of CAS (Grant No. KLSMS-1405).

Competing interests

The authors declare that they have no competing interests.

References

- [1] H. Raether, Surface Plasmons on Smooth and Rough Surfaces and on Gratings, Springer-Verlag, (1988).
- [2] L. Martin-Moreno, F. J. Garcia-Vidal, H. J. Lezec, A. Degiron, T. W. Ebbesen, Phys. Rev. Lett. **90**, 167401 (2003).
- [3] S. I. Bozhevolnyi, V. S. Volkov, E. Devaux, T. W. Ebbesen, Phys. Rev. Lett. **95**, 046802 (2005).
- [4] I. Avrutsky, R. Soref, W. Buchwald, Opt. Express **18**, 348 (2010).
- [5] Y. S. Bian, Q. H. Gong, Laser Photon Rev. **8**, 549 (2014).
- [6] D. X. Dai, S. L. He, Opt. Express **17**, 16646 (2009).
- [7] R. F. Oulton, G. Bartal, D. F. P. Pile, X. Zhang, New J. Phys. **10**, 105018 (2008).
- [8] W. L. Barnes, A. Dereux, T. W. Ebbesen, Nature **424**, 824 (2003).
- [9] E. Ozbay, Science **311**, 189 (2006).
- [10] M. Staffaroni, J. Conway, S. Vedantam, J. Tang, E. Yablonovitch, Photon. Nanostruct. **10**, 166 (2012).
- [11] H. Choo, M. K. Kim, M. Staffaroni, T. J. Seok, J. Bokor, S. Cabrini, P. J. Schuck, M. C. Wu, E. Yablonovitch, Nat. Photon. **6**, 837 (2012).
- [12] O. Hess, J. B. Pendry, S. A. Maier, R. F. Oulton, J. M. Hamm, K. L. Tsakmakidis, Nat. Mater. **11**, 573 (2012).

- [13] M. T. Hill, Y. S. Oei, B. Smalbrugge, Y. Zhu, T. De Vries, P. J. Van Veldhoven, F. W. M. Van Otten, T. J. Eijkemans, J. P. Turkiewicz, H. De Waardt, E. J. Geluk, S. H. Kwon, Y. H. Lee, R. Notzel, M. K. Smit, *Nat. Photon.* **1**, 589 (2007).
- [14] J. N. Anker, W. P. Hall, O. Lyandres, N. C. Shah, J. Zhao, R. P. Van Duyne, *Nat. Mater.* **7**, 442 (2008).
- [15] P. Berini, I. De Leon, *Nat. Photon.* **6**, 16 (2012).
- [16] R. F. Oulton, V. J. Sorger, D. A. Genov, D. F. P. Pile, X. Zhang, *Nat. Photon* **2**, 496 (2008).
- [17] T. Y. Huang, P. M. Tagne, S. N. Fu, *Opt. Express* **24**, 9706 (2016).
- [18] W. Wei, X. Zhang, H. Yu, X. Ren, *Photon. Nanostruct.* **11**, 279 (2013).
- [19] J. Wang, L. Sun, Z. D. Hu, X. Liang, C. Liu, *AIP Advances* **4**, 123006 (2014).
- [20] R. A. Wahsheh, M. A. G. Abushagur, *Opt. Express* **24**, 8237 (2016).
- [21] Y. S. Bian, Z. Zheng, X. Zhao, Y. L. Su, L. Liu, J. S. Liu, J. S. Zhu, T. Zhou, *Journal of Optics* **15**, 055011 (2013).
- [22] Z. X. Chen, Z. J. Wu, Y. Ming, X. J. Zhang, Y. Q. Lu, *AIP Advances* **4**, 017103 (2014).
- [23] Z. Zheng, Y. Bian, X. Zhao, Y. L. Su, L. Liu, J. S. Liu, J. S. Zhu, T. Zhou, *IEEE J. Sel. Top. Quantum Electron.* **19**, 4800106 (2013).
- [24] E. Moreno, F. J. Garcia-Vidal, S. G. Rodrigo, L. Martin-Moreno, S. I. Bozhevolnyi, *Opt. Lett.* **31**, 3447 (2006).
- [25] A. Vakil, N. Engheta, *Science* **332**, 1291 (2011).
- [26] D. K. Gramotnev, K. C. Vernon, *Appl. Phys. B* **86**, 7 (2007).
- [27] Z. Q. Li, E. A. Henriksen, Z. Jiang, Z. Hao, M. C. Martin, P. Kim, H. L. Stormer, D. N. Basov, *Nat. Phys.* **4**, 532 (2008).
- [28] D. K. Efetov, P. Kim, *Phys. Rev. Lett.* **105**, 256805 (2010).
- [29] C. Ding, R. Yu, H. Xiong, X. Yang, Y. Wu, *J. Appl. Phys.* **115**, 234301 (2014).
- [30] L. Ju, B. Geng, J. Horng, C. Girit, M. Martin, Z. Hao, H. A. Bechtel, X. Liang, A. Zettl, Y. R. Shen, F. Wang, *Nat. Nanotechn.* **6**, 630 (2011).
- [31] B. Wang, X. Zhang, X. C. Yuan, J. H. Teng, *Appl. Phys. Lett.* **100**, 131111 (2012).
- [32] B. Wang, X. Zhang, F. J. Garcia-Vidal, X. C. Yuan, J. H. Teng, *Phys. Rev. Lett.* **109**, 073901 (2012).
- [33] H. S. Chu, C. H. Gan, *Appl. Phys. Lett.* **102**, 231107 (2013).
- [34] T. Low, P. Avouris, *ACS Nano* **8**, 1086 (2014).
- [35] D. Ansell, I. P. Radko, Z. Han, F. J. Rodriguez, S. I. Bozhevolnyi, A. N. Grigorenko, *Nat. Communications* **6**, 8846 (2015).
- [36] J. Guo, L. Y. Jiang, X. Y. Dai, Y. J. Xiang, *Opt. Express* **24**, 4740 (2016).
- [37] Z. Y. Fang, S. Thongrattanasiri, A. Schlather, Z. Liu, L. L. Ma, Y. M. Wang, P. M. Ajayan, P. Nordlander, N. J. Halas, F. Javier Garcia de Abajo, *ACS Nano* **7**, 2388 (2013).
- [38] P. H. Liu, X. Z. Zhang, Z. H. Ma, W. Cai, L. Wang, J. J. Xu, *Opt. Express* **21**, 32432 (2013).
- [39] Y. X. Gao, G. B. Ren, B. F. Zhu, H. Q. Liu, Y. D. Lian, S. S. Jian, *Opt. Express* **22**, 24322 (2014).
- [40] X. He, X. Zhang, H. Zhang, M. Xu, *IEEE J. Sel. Top. Quantum Electron.* **20**, 4500107 (2014).
- [41] W. Li, B. Chen, C. Meng, W. Fang, Y. Xiao, X. Li, Z. Hu, Y. Xu, L. Tong, H. Wang, W. Liu, J. Bao, Y. R. Shen, *Nano Lett.* **14**, 955 (2014).
- [42] J. M. Jin, *The Finite Element Method in Electromagnetics*, Wiley-IEEE Press, New York (2002).

*Corresponding author: jcwang@jiangnan.edu.cn